Burning Velocity and OH Concentration in Premixed Combustion

by

K. Yamamoto, M. Ozeki, N. Hayashi, and H. Yamashita
Department of Mechanical Science and Engineering, Faculty of Engineering, Nagoya University
Furo-cho, Chikusa-ku, Nagoya-shi, Aichi 464-8603, JAPAN

(Abstract)

In the present paper, we have simulated laminar premixed flames in several types of flow configuration. The counter-flow flame, 1D flame in uniform flow, and 2D flame on a slot burner have been considered. The fuel is propane, and detailed chemistry has been used. We have obtained burning velocity in these flames to examine the response of peak OH concentration in flame zone to burning velocity (S_L). In case of counter-flow flame, peak OH concentration is decreased at the larger stretch rate. At the same time, the burning velocity is decreased. The peak OH concentration of 1D flame in uniform flow is decreased at lower equivalence ratio, with smaller burning velocity. It is interesting to note that, for both flames as well as 2D flame, the same linear relationship is observed between two parameters of peak OH and S_L. Thus, consistent with earlier findings of turbulent flames, peak OH concentration can be a good measure of burning velocity. In the experiments, we have estimated local burning velocity in turbulent combustion with a cyclone-jet combustor. The slot burner has been used for calibration. It is found that the peak OH concentration in the flame becomes smaller with an increase of turbulence. In some cases, its value is almost zero, which could be local extinction. The local burning velocity is monotonically decreased at higher turbulence. When the fuel is propane, Markstein number is positive for lean mixture. In that case, the burning velocity is decreased due to the stretch effect, which is well in accordance with the fact that the turbulence always suppresses the burning velocity in our measurements.

INTRODUCTION

In turbulent combustion, eddies move randomly back and force across the flame region, and there is a strong interaction between flames and flow. It is useful to consider the elementary laminar flames such as counter-flow flames [1-7] and a tubular flame [8-12]. These flame configurations are of great interest, because it is possible to conduct one-dimensional calculations, and hence, the detailed chemical reactions and multi-component transport properties are easy to use in the simulation. So far, effects of strain rate, equivalence ratio, and temperature on the flame have been investigated. Since the tubular flame is formed in an axis-symmetric stretched and rotating flow field, the effect of rotation on the flame structure has been successfully clear, which is explained with pressure diffusion and flame stretch caused by the centrifugal force in rotation [10-12].

For the design of practical combustors and furnaces, burning velocity is one of the most important flame characteristics, which is related with chemical reaction and heat release rate. In case of turbulent combustion, due to rapid mixing and increased heat and mass transfer, combustion rate is expectedly enhanced, resulting in a large turbulent burning velocity. In early studies, Damköhler [13] has proposed that, when the flame only wrinkles with turbulence, the turbulent burning velocity, S_T, is expressed by

$$S_T = (A_T / A_L) S_L \qquad (1)$$

where A_T is the surface area of the wrinkled flame front, and A_L is the cross-sectional area of the front projected in the direction of flame propagation. That is, the increase of flame surface area enlarges the apparent burning velocity without any change in the instantaneous local flame structure. This unsteady flame behavior is important for discussing combustion noise, combustion instabilities, and pulsed combustion.

However, there are few fundamental researches on the estimation of local burning velocity

(displacement speed of flame front) in turbulent combustion, because the direct measurement is difficult experimentally. We need 3D information of both velocity field and flame motion with high resolution of time and space. Ronney et al. have experimentally examined the aqueous autocatalytic reactions to discuss local reaction and burning velocity [14-16]. Although the improvement of computer simulations has been drastically progressed [17,18], due to the huge calculation time, it is more or less impractical to conduct 3D simulation with detailed chemistry.

In this study, using detailed chemistry, we simulate the fundamental flames such as the counter-flow flame, 1D flame in uniform flow, and 2D flame on a slot burner [19]. By considering different flame configurations, we investigate OH concentration and the burning velocity. Based on the response of OH concentration to the burning velocity, we estimate the local burning velocity in turbulent combustion with a cyclone-jet combustor [20,21]. A planar laser-induced fluorescence technique (PLIF) has been applied to obtain OH concentration [22-25]. For calibration of absolute OH concentration, comparison of numerical and experimental results is made.

NUMERICAL APPROACH

Figure 1 shows flame configurations considered in this study, including 1D flame in uniform flow (**Fig. 1(a)**), counter-flow flame (**Fig. 1(b)**), and 2D flame on a slot burner (**Fig. 1(c)** as well as **Fig.2**). The model, assumptions, and numerical techniques are almost the same with those of our previous studies [26-28], except for the chemical scheme. As for the counter-flow flame, the details for numerical approach are explained in recent papers [29,30]. The conservation equations of mass, momentum, energy, and species were solved by a finite volume method. For these time-dependent conservation equations, the time advance was performed until the steady state was achieved. All calculations were carried out at atmospheric pressure and room

temperature. Mixture is an ideal gas. The Soret effect, the Dufour effect, the pressure diffusion, and the viscous energy dissipation were ignored. The thermodynamic properties for the species are obtained from the CHEMKIN database [31]. The transport properties were calculated according to a Smooke's simplified transport model [32]. The detailed chemistry of the GRI-Mech 3.0 [33] was used, containing 53 species and 325 elementary reactions.

The calculation conditions especially for counter-flow premixed flame are explained here. It is 1D simulation using similarity solution along the coordinate of x-direction in **Fig. 1(b)**. To consider the Bunsen-type flame or turbulent jet premixed flame in surrounding air, opposed jets of premixed gas and air were considered. The distance of D between inlets of these flows is 15 mm, with 200 uniform grid points. The fuel is propane. The velocity of both jets, U, was changed to vary the global stretch rate in the flow, κ (=$2U/D$). In the simulation, the global stretch rate is between 50 to 350 1/s, where the steady flame is formed.

EXPERIMENTAL

Cyclone-jet combustor and slot burner

Figure 2 (upper figure) shows a cyclone-jet combustor (C-J combustor). With the C-J combustor, it is possible to investigate turbulent flames over a wide range of turbulent properties [20,21]. It consists of a combustion chamber with a main jet nozzle and two cyclone nozzles for pilot flames. The diameter of the main jet nozzle is 12.7 mm and that of the cyclone combustor is 21 mm, with two cyclone nozzles of 2.4 mm i.d. Since the flame is stabilized at the combustor exit, it is easy to conduct PLIF measurements. In the experiment, we varied the mean velocity at the combustor exit, U_m, and the equivalence ratio, ϕ_m, of the main jet, with a fixed condition of pilot flames for U_p = 20 m/s and ϕ_p = 0.7. The fuel is propane. The turbulent Reynolds number, Re_T, is from 96 to 448 for U_m = 5 to 30 m/s, ϕ_m = 0.75 and 0.9. On the phase diagram, the

condition of U_m < 15 m/s for ϕ_m = 0.75 or U_m < 20 m/s for ϕ_m = 0.90 belongs to the flamelet regime, and that of U_m > 20m/s for ϕ_m = 0.75 or U_m = 30 m/s for ϕ_m = 0.90 belongs to the thin reaction zones regime. Here, Z represents the axial distance from the combustor exit and Y is the horizontal axis. To obtain the absolute OH concentration, a slot burner in **Fig. 2 (lower figure)** was used [19]. The velocity is 1m/s and the equivalence ratio is 0.9, corresponding to the flow configuration in **Fig. 1(c),** so that we compare the OH fluorescence signal with simulated OH profile for calibration.

OH-PLIF system

To measure the OH concentration, a PLIF technique was applied. The experimental setup is shown in **Fig. 3**. The beam of a pulsed laser was used to form a thin laser sheet for 2D flame images. A Nd:YAG-pumped dye laser is frequency doubled to 283.2 nm to excite OH with $Q_1(7)$ line in the 1-0 band of the A-X transition. The laser energy is about 10 mJ at 283.2 nm. The fluorescence from OH was measured with a gated image-intensified CCD camera. The laser beam thickness is less than 0.5 mm, and the resolution of the camera is 0.1mm. The image size shown in **Fig. 2** is 26 mm × 5 mm at Z = 17.5 to 22.5 mm, and 500 images were obtained for statistical analysis. As already explained, a slot burner was used to form a stable laminar flame for calibration. Since the flame height is short, we obtained LIF signals at Z = 7.5 to 12.5 mm.

In this measurement, it is confirmed that the laser intensity for OH excitation is not in the saturation regime. Then, molar OH concentration is described by the fluorescence signal as

$$[\mathrm{OH}] = aC_gC_qI / L \qquad (2)$$

where a is the constant including the collection efficiency in LIF system, I is the fluorescence intensity, and L is the laser intensity. The ground state correction factor, C_g, is the ratio of the number density of molecules at

the ground state in selected excitation line to the total number density. **Figure 4(a)** shows the temperature dependence of ground state correction factor in the $Q_1(7)$ line [34]. As already reported, C_g has only small temperature dependence, less than 10 % in the range of 1000 K to 2000 K.

On the other hand, the electronic quenching correction factor, C_q, is expressed by

$$C_q = \frac{A}{A+Q} \approx \frac{A}{Q} \qquad (3)$$

where A is the Einstein emission coefficient and Q is the quenching rate, both in 1/s units. In order to examine the temperature dependence of C_q, we evaluated the quenching rate [34,35].

$$Q = \sum_i \sigma_i \bar{v}_i n_i \qquad (4)$$

Here, σ_i and n_i are the cross section and number density for species i. Also, $\bar{v}_i$ is the mean velocity given by

$$\bar{v}_i = \sqrt{\frac{8kT}{\pi \mu_i}} \qquad (5)$$

where k is the Boltzmann constant and μ_i is the reduced mass between species i and OH. Then, Q can be determined if the temperature and concentration profiles are known. In preliminary simulation of 1D flame in **Fig. 1(a)**, we estimated quenching rate in propane/air mixture. Since OH exists in the temperature range of 900 K < T, only major species of O_2, N_2, CO_2, CO, H_2O, and H_2 were included for collision quenching. The harpoon model was used to determine the cross section of these species [36]. **Figure 4(b)** shows the

calculated quenching rate with temperature. The equivalence ratio is 0.75 and 0.90. The temperatures where OH concentration becomes the peak value are 1740 K for $\phi = 0.75$ and 1850 K for $\phi = 0.90$. It is found that the small temperature dependence is observed, so that the absolute OH concentration is obtained by considering that the fluorescence signal is simply proportional to OH concentration.

RESULTS AND DISCUSSION

Simulation of laminar flames

Figure 5 shows the simulated OH concentration of 1D flame in uniform flow. The equivalence ratio is set to be 0.7, 0.75, 0.8, 0.9, and 1.0. In the simulation, we changed the inlet velocity to stable the flame at the position of $x = 0$. When the steady state is achieved, the inlet velocity is equal to the so-called laminar burning velocity. As seen in this figure, there is a peak OH concentration, which is the super-equilibrium value in flame region. At the far downstream, its concentration becomes the equilibrium value. From this figure, we can examine the relationship between peak OH concentration and burning velocity, which will be given later to compare all results of different flame configurations.

Next, we show results of counter-flow flames. To simulate the flame at different stretch rate, the inlet velocity was changed. Some examples at the equivalence ratios of 0.9 and 1.0 are shown in **Fig. 6**. The peak OH concentration and the burning velocity are plotted as functions of global stretch rate. Here, the burning velocity was obtained by the integration of reaction rate [37]. As seen in this figure, as the stretch rate is increased, the peak OH concentration in the flame region is gradually decreased. Then, the flame extinction is observed. The burning velocity is also decreased with an increase of stretch rate.

According to Becker et al., it has been pointed out that the peak OH concentration in turbulent flames is a good measure of the strength of chemical activity in the reaction region [22]. Recently, the excellent

correlation between OH and local burning velocity has been reported in the simulation of turbulent flames [38]. To confirm this relationship, we examined these two parameters in counter-flow flames. All the computed data are plotted in **Fig. 7**. The equivalence ratios are 0.8, 0.9 and 1.0. When the equivalence ratio was set to be below 0.75, the steady flame was not formed. For comparison, those of 1D flame in uniform flow and 2D flame on a slot burner are shown in this figure. Surprisingly, a good linear relationship is observed between peak OH concentration and burning velocity even at the different equivalence ratio. Especially, in counter-flow flames, this linearity is observed at different strain rate (up to 350 1/s). Although the theoretical explanation is not clear, it can be concluded that OH concentration is a good marker to evaluate the burning velocity.

Measurements of laminar and turbulent flames

Finally, in experiments, we estimated the burning velocity based on peak OH concentration. First, we need to obtain the absolute OH concentration. **Figures 8(b)-(d)** show the instantaneous OH fluorescence images of turbulent flames at U_m = 5, 20, and 30 m/s for ϕ_m = 0.90. The OH image of a laminar flame on the slot burner is also shown in **Fig. 8(a)**. These signals are divided by the laser intensity, L, to compensate for laser profile fluctuations. In case of the laminar flame, the flame is flat and the fluorescence signal is almost constant along the flame front. On the other hand, OH profile in a cyclone-jet combustor is always fluctuating. When the exit velocity is increased, the wrinkle of the flame front becomes complex. It is interesting to note that, OH region is distributed at U_m = 30 m/s, with the fluorescence signal weaker. The turbulent flame in the cyclone-jet combustor is always stabilized on the combustor exit. Then, it is expected that the flame front could be detected in OH image, because 2D laser sheet is across the flame front. In Ref. 39, we have confirmed that the reduction of OH signal in highly turbulent case is due to the local extinction.

Here, we explain the procedure to determine molar OH concentration, [OH], in the slot burner. The

comparison of fluorescence signals and numerical results with the same burner geometry and flow conditions are shown in **Fig. 9**. These profiles are obtained at $Z = 10$ mm at $\phi = 0.9$. The direct photograph of the flame is shown in this figure. Although some discrepancies are observed in the burned gas region in surrounding air, the agreement is good around the blue flame region in the photograph. For calibration, it is considered that peak (maximum) OH fluorescence signal is matched with the peak (maximum) molar OH concentration in this figure, and the absolute OH concentration in turbulent flames is calculated by

$$[\mathrm{OH}] = \frac{(I/L)}{(I/L)_{max,Laminar}}[\mathrm{OH}]_{max,Laminar} \qquad (6)$$

This equation provides the OH concentration in the flame, ensuring that the flame characteristics are quantitatively discussed based on OH concentration. Although Eq.6 may not be appropriate when the local flame extinction occurs, its symptom appears in OH concentration in the qualitative way.

Figure 10 shows the averaged value of the peak OH concentration, which is obtained at $Z = 20$ mm in each LIF image of turbulent flames. The equivalence ratios are 0.75 and 0.9. In this figure, the measured maximum and minimum of peak OH concentrations are shown by error bar. The OH concentration of a laminar flame for $\phi = 0.90$ is also plotted. As seen in this figure, peak OH concentration largely fluctuates even for $U_m = 5$ m/s. At higher equivalence ratio, OH concentration is expectedly larger. As the exit velocity is increased, the averaged peak OH concentration is monotonically decreased. It is interesting to note that, in some cases at $U_m = 20$ or 30 m/s for $\phi_m = 0.75$, OH concentration is close to zero. Although other radicals may be present, our recent measurements have shown that the heat release rate is almost zero in this case [39]. Then, it is considered that the local extinction could occur, where combustion reaction can not be sustained in highly turbulent combustion.

Figure 11 shows the local burning velocity calculated by the measured peak OH concentration based on the linear relationship in **Fig. 7**. This is the probability density function (PDF) of burning velocity for both equivalence ratios at Z = 20 mm. For comparison, the laminar burning velocity in unstrained uniform flow, S_L^0, is shown. For both cases, as the turbulence is larger at higher exit velocity, the distribution is shifted toward the lower burning velocity. Additionally, the local burning velocity is always below S_L^0. It should be noted that, in some cases highly observed for 30 m/s, S_L becomes zero, corresponding to the local extinction. To discuss the burning velocity of turbulent flames affected by the stretched effect, it is useful to consider the Markstein number [40,41]. When the fuel is propane, Markstein number is positive for lean mixture. It is known that the burning velocity is reduced due to the stretch effect, which is well observed in our measurements.

CONCLUSIONS

We have simulated laminar premixed flames in several types of flow configuration. The counter-flow flame, 1D flame in uniform flow, and 2D flame on a slot burner have been considered. The fuel is propane, and detailed chemistry has been used. We have examined the response of peak OH concentration to the burning velocity (S_L) of these flames. In the experiments, based on the relationship between peak OH and S_L, we have estimated local burning velocity in turbulent combustion with a cyclone-jet combustor. The following conclusions are made.

(1) In the case of counter-flow flame, peak OH concentration is decreased at the larger stretch rate. At the same time, the burning velocity is decreased. The peak OH concentration of 1D flame in uniform flow is decreased at lower equivalence ratio, with smaller burning velocity. For both flames as well as 2D flame, the same linear relationship is observed between these two parameters of peak OH and S_L. Thus,

consistent with earlier findings of turbulent flames, OH concentration can be a good measure of burning velocity.

(2) In turbulent combustion, the peak OH concentration becomes smaller with an increase of turbulence. In some cases, its value is almost zero, which could be local extinction. The local burning velocity is monotonically decreased. Since Markstein number is positive for lean propane/air mixture, these results are well in accordance with the theoretical explanation that the burning velocity is reduced due to the stretch effect.

REFERENCES

1. Tsuji, H., and Yamaoka, I., *Proc. Comb. Inst. 19*, (1982), pp. 1533-1540.

2. Sato, J., *Proc. Comb. Inst. 19*, (1982), pp. 1541-1548.

3. Matalon, M., *Combust. Sci. Tech., Vol. 31*, (1983), pp. 169-181.

4. Mizomoto, M., Asaka,Y., Ikai, S. and Law, C. K., *Proc. Comb. Inst. 20*, (1984), pp. 1933-1939.

5. Law, C. K., Cho, P., Mizomoto, M. and Yoshida, H., *Proc. Comb. Inst. 21*, (1986), pp. 1803-1809.

6. Chung, S. H. and Law, C. K., *Combust. Flame 55*, (1984), pp. 123-125.

7. Ju, Y., Masuya, G., Liu, F., Guo, H., Maruta, K., and Niioka, T., *Proc. Comb. Inst. 27*, (1998), pp. 2551-2557.

8. Ishizuka, S., *Proc. Comb. Inst. 20*, (1984), pp. 287-294.

9. Nishioka, M., Takeno, T., Ishizuka, S., *Combust. Flame 73*, 287-301 (1988).

10. Yamamoto, K., Ishizuka, S. and Hirano, T., *Proc. Comb. Inst. 26*, (1996), pp. 1129-1135.

11. Yamamoto, K., *Combust. Flame 118*, 431-444 (1999).

12. Zhang, Y., Ishizuka, S., Zhu, H., and Kee, R. J., *Proc. Comb. Inst.* 31, (2007), pp. 1101-1107.

13. Damköhler, G., Z. Elektrochem. Angew. *Phys. Chem* 46 (1940) 601-626.

14. Shy, S. S., Ronney, P. D., Buckley, S. G., and Yakhot, V., *Proc. Comb. Inst. 24*, (1992), pp. 543-551.

15. Ronney, P. D., Haslam, B. D., and Rhys, N. O., *Physical Review Letters, 24(19)*, (1995), pp. 3804-3807.

16. Shy, S. S., Jang, R. H., and Ronney, P. D., *Combust. Sci. Tech., 113-114*, (1996), pp. 329-350.

17. Tanahashi, M., Fujimura, M., and Miyauchi, T., *Proc. Combust. Inst.* 28 (2000) 529-535.

18. Bell, J. B., Dat, M. S., and Grcar, J. F., *Proc. Combust. Inst.* 29 (2002) 1987-1993.

19. Rosen L. J., and Axelbaum, R. L., *Combust. Flame* 126 (2001) 1433-1444.

20. Yamamoto, K., Nishizawa, Y., and Onuma, Y., *JSME Int. J, Series B* 47- 6 (2003) 408-415.

21. Yamamoto, K., Inoue, S., Yamashita, H., Shimokuri, D., Ishizuka, S., and Onuma, Y., *Heat Transfer Asian Research*, 35 (2006) 501-512.

22. Becker, H., Monkhouse, P. B., Wolfrum, J., Cant, R. S., Bray, K. N. C., Maly, R., Pfister, W., Stahl, G., and Warnatz, J., *Proc. Combust. Inst.* 23 (1990) 817-823.

23. Smooke, M. D., Xu, Y., Zurn, R. M., Lin, P., Frank, J. H., and Long, M. B., *Proc. Comb. Inst. 24*, (1992), pp. 813-821.

24. Yamamoto, K., Ishizuka, S., and Hirano, T., *Proc. Combust. Inst.* 25 (1994) 1399-1406.

25. Buschmann, A., Dinkelacker, F., Schafer, T., and Wolfrum, J., *Proc. Combust. Inst.* 26 (1996) 437-445.

26. Yamashita, H., Kushida, G., and Takeno, T., *Proc. R. Soc. London, Ser. A*, 431: 301-314 (1990).

27. Yamashita, H., Kushida, G., and Takeno, T., *Proc. Combust. Inst.* 24 (1992) 311-316.

28. Yamashita, H., Shimada, M., and Takeno, T., *Proc. Combust. Inst.* 26 (1996) 27-34.

29. Zhao, D., Yamashita, H., Kitagawa, K., Arai, N., and Furuhata, T., *Combust. Flame* 130: 352-360 (2002).

30. Yamamoto K., et al., *J. Combustion Society of Japan*, 49-149: 181-186 (2007).

31. Kee, R. J. , Rupley, F. M. and Miller, J. A., Sandia National Laboratories Report No. SAND89-8009, 1989.

32. Smooke, M. D., *Reduced Kinetic Mechanisms and Asymptotic Approximations for Methane-Air Flames*, Springer-Verlag, Berlin, Germany, 1991.

33. http://www.me.berkeley.edu/gri_mech/version30/text30.html.

34. Horie, R., Ito, A., Nishioka M., Zhu, X. L., and Takeno T., *Trans. Japan Society for Mechanical Eng*. B65 (1999) 54-61.

35. Garland, N. L., and Crosley, D. R., *Proc. Combust. Inst.* 21 (1986) 1693-1702.

36. Paul, P. H., *J. Quant. Spectrosc. Radiat. Transfer* 51 (1994) 511-524.

37. Poinsot, T., Veynante, D., and Candel, S., *J. Fluid Mech.* 228 (1991) 561-606.

38. Bell, J. B., Cheng, R. K., Day, M. S., and Shepherd, I. G., *Proc. Combust. Inst.* 31 (2007) 1309-1317.

39. Ohnishi, M. Ishii, S., Yamamoto, K., Hayashi, N., Yamashita, H., *Proc. Sixth Asia-Pacific Conference on Combustion* (2007), 340-343.

40. Tseng, L. -K., Ismal, M. A., and Faeth, G. M., *Combust. Flame* 95: 410-426 (1993).

41. Davis, S. G., Quinard, J., and Searby, G., *Combust. Flame*, 130 (2002), 123-136.

List of figure captions

Figure 1 Flame configurations considered in this study.

Figure 2 Cyclone-jet combustor (upper) and slot burner (lower).

Figure 3 Experimental setup for OH-PLIF system.

Figure 4 (a) Temperature dependence of ground state correction factor in the $Q_1(7)$ line, (b) quenching rate as functions of temperature in simulation using GRI-Mech 3.0.

Figure 5 OH profiles of 1D flame in uniform flow at the equivalence ratio of 0.7, 0.75, 0.8, 0.9 and 1.0. There is a peak OH concentration of super-equilibrium value in flame region. At downstream, its concentration becomes equilibrium value.

Figure 6 Peak OH concentration and burning velocity of counter-flow flames for $\phi = 0.9$ and 1.0.

Figure 7 Relationship between peak OH concentration and burning velocity in counter-flow premixed flame for propane/air mixtures. All the computed data of 1D flame in uniform flow and laminar flame on a slot burner are plotted.

Figure 8 Fluorescence obtained by LIF system; (a) slot burner, (b)-(d) cyclone-jet combustor for $\phi_m = 0.90$.

Figure 9 Profiles of LIF signals and simulated OH concentration of flame on a slot burner; $Z = 10$ mm, $\phi = 0.9$.

Figure 10 Variations of peak OH concentration with exit velocity. Measured maximum and minimum are shown by error bar.

Figure 11 PDF of local burning velocity for (a) $\phi_m = 0.75$ and (b) $\phi_m = 0.90$. For comparison, the laminar burning velocity, S_L^0, is shown by dotted line.

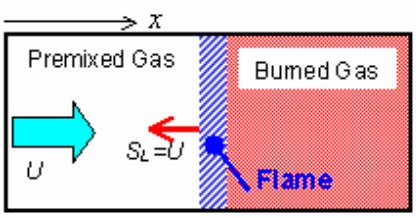

(a) 1D flame in uniform flow

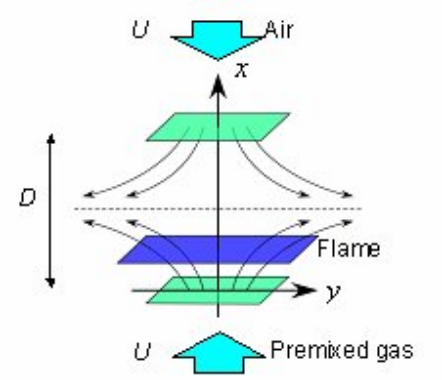

(b) Counter-flow flame in opposed jets of premixed gas and air

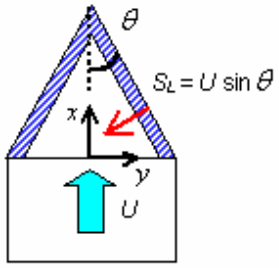

(c) 2D flame on a slot burner

Figure 1 Flame configurations considered in this study.

[Word Count] = (160+10)*2.2*1 + 8 (caption) = 382 words

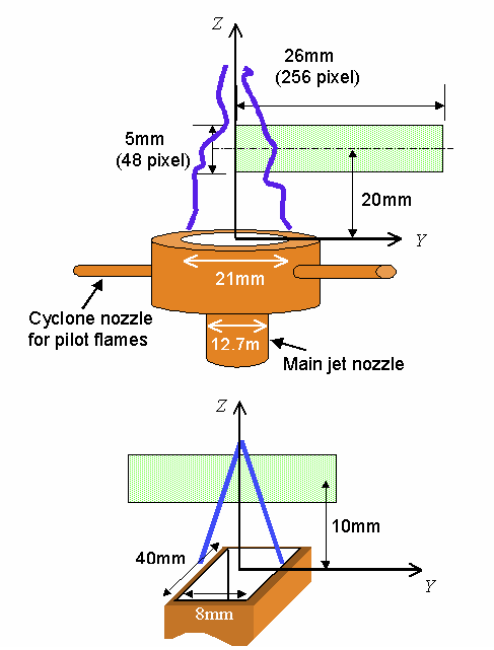

Figure 2 Cyclone-jet combustor (upper) and slot burner (lower).

[Word Count] = (85+10)*2.2*1 + 9 (caption) = 218 words

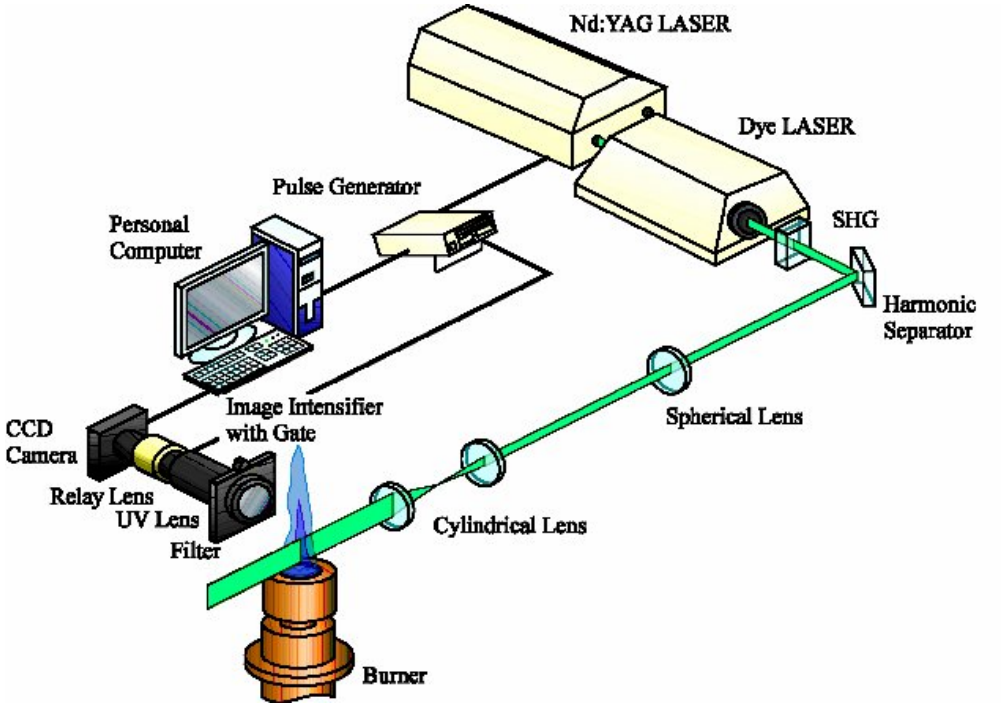

Figure 3 (enlarged)

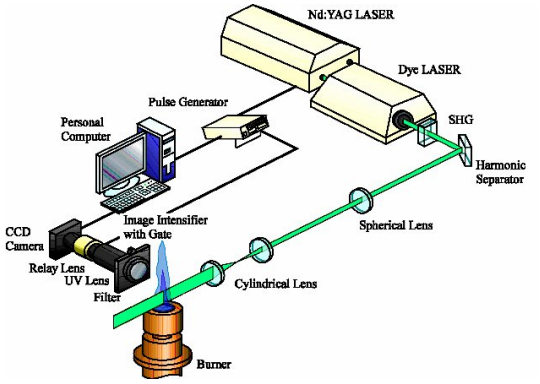

Figure 3 Experimental setup for OH-PLIF system.

[Word Count] = (50+10)*2.2*1 + 7 (caption) = 139 words

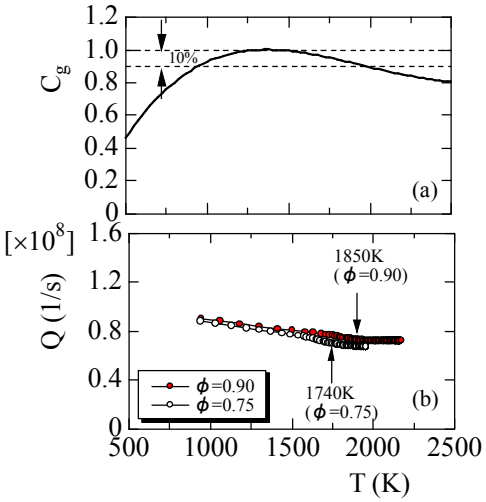

Figure 4 (a) Temperature dependence of ground state correction factor in the $Q_1(7)$ line, (b) quenching rate as functions of temperature in simulation using GRI-Mech 3.0.

[Word Count] = (65+10)*2.2*1 + 26 (caption) = 194 words

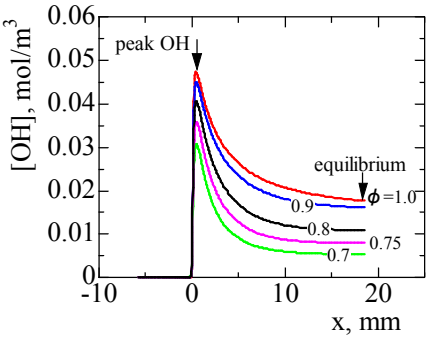

Figure 5 OH profiles of 1D flame in uniform flow at the equivalence ratio of 0.7, 0.75, 0.8, 0.9 and 1.0. There is a peak OH concentration of super-equilibrium value in flame region. At downstream, its concentration becomes equilibrium value.

[Word Count] = (45+10)*2.2*1 + 40 (caption) = 161 words

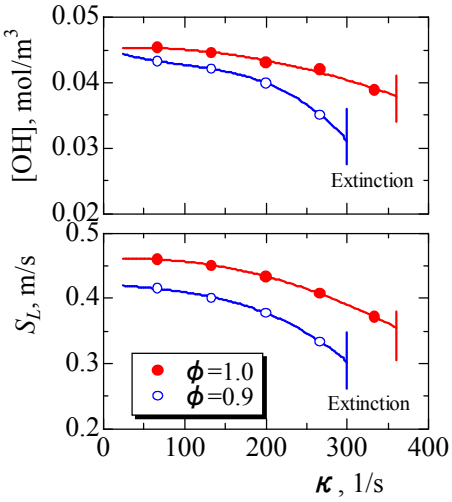

Figure 6 Peak OH concentration and burning velocity of counter-flow flames for $\phi = 0.9$ and 1.0.

[Word Count] = (65+10)*2.2*1 + 17 (caption) = 182 words

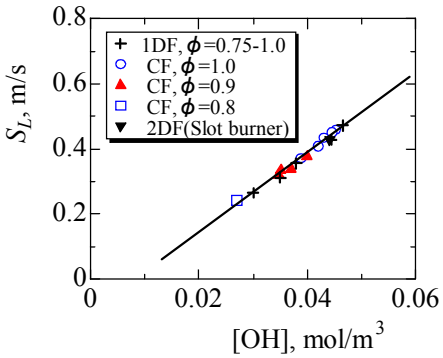

Figure 7 Relationship between peak OH concentration and burning velocity in counter-flow premixed flame for propane/air mixtures. All the computed data of 1D flame in uniform flow and laminar flame on a slot burner are plotted.

[Word Count] = (45+10)*2.2*1 + 34 (caption) = 181 words

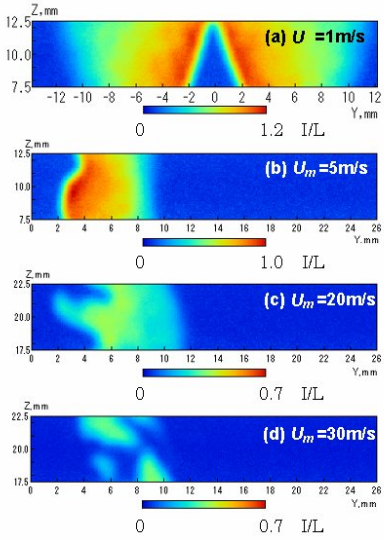

Figure 8 Fluorescence obtained by LIF system; (a) slot burner, (b)-(d) cyclone-jet combustor for $\phi_m = 0.90$.

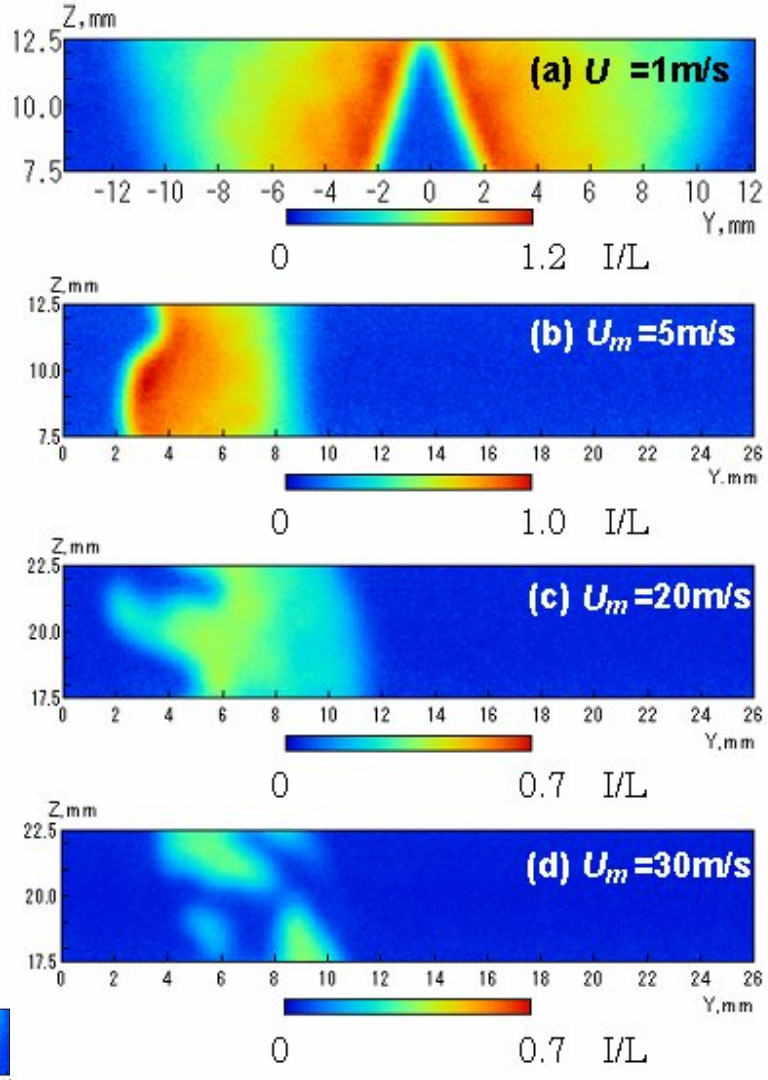

Fig.8 (enlarged)

[Word Count] = (70+10)*2.2*1 +13 (caption) = 189 words

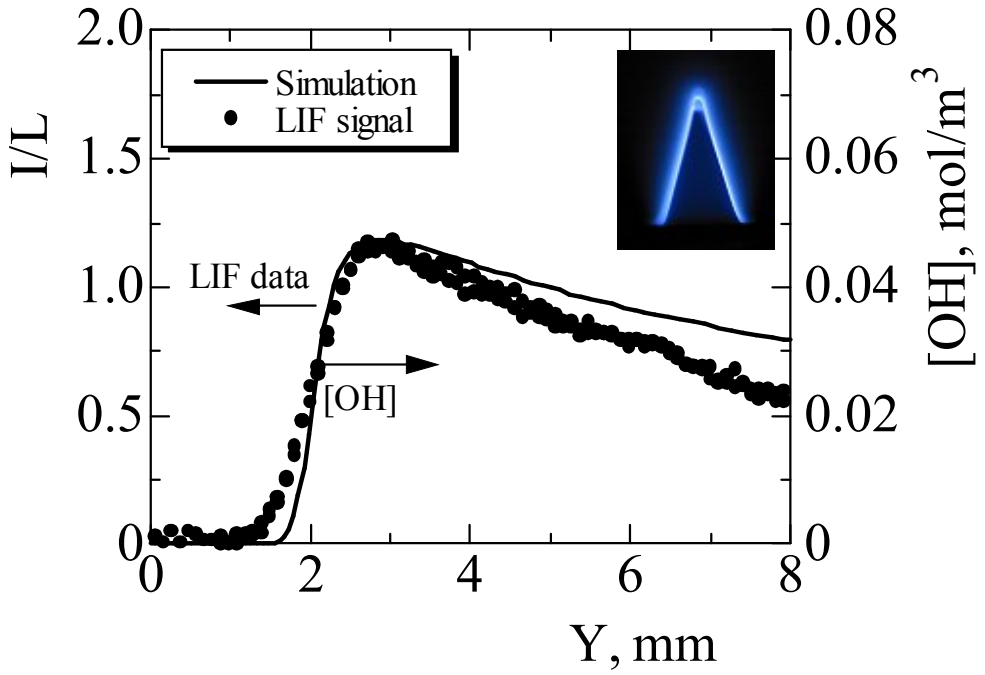

Figure 9 (enlarged)

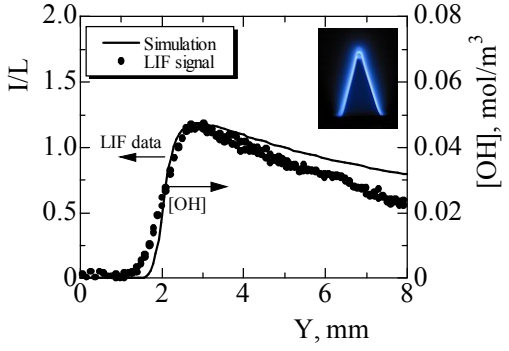

Figure 9 Profiles of LIF signals and simulated OH concentration of flame on a slot burner; $Z = 10$ mm, $\phi = 0.9$.

[Word Count] = (45+10)*2.2*1 + 22 (caption) = 143 words

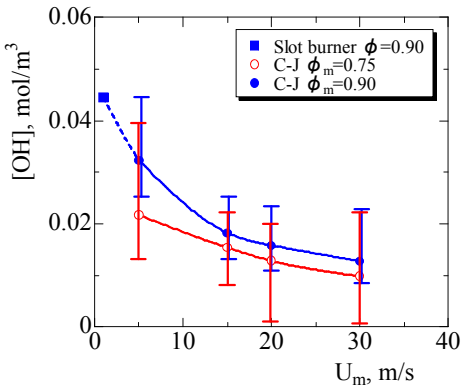

Figure 10 Variations of peak OH concentration with exit velocity. Measured maximum and minimum are shown by error bar.

[Word Count] = (50+10)*2.2*1 + 19 (caption) = 151 words

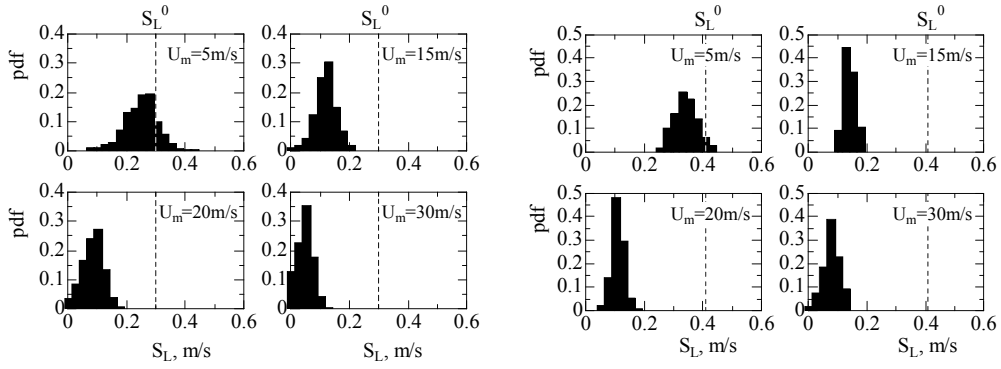

(a) $\phi_m = 0.75$ (b) $\phi_m = 0.90$

Figure 11 PDF of local burning velocity for (a) $\phi_m = 0.75$ and (b) $\phi_m = 0.90$. For comparison, the laminar burning velocity, S_L^0, is shown by dotted line.

[Word Count] = (55+10)*2.2*2 + 28 (caption) = 314 words